UNIVERSITY OF TWENTE

# Mathematical modeling to better understand the dynamics of epilepsy

Miriam Jonkheer

December 23, 2016

## 1 ABSTRACT

Recently a lot of research has been conducted to increase the understanding of the brain dynamics, particularly regarding abnormal behavior. One of the most common neurological disorders is epilepsy and is therefore an important research topic. However, so far this disorder has only been theoretically characterized as being associated with abnormal synchronization between brain regions. Therefore Schmidt et al. (2014) tested a new method for analyzing this synchronization. For this they used the Kuramoto model. This model is said to be a good way of modeling the brain dynamics associated with epilepsy. Using this model they found markers to distinguish between healthy subjects and epilepsy patients using rest-EEGs. This research was conducted to confirm their findings. This study has indeed found a reduction in the critical coupling strength required to synchronize the global network in the low-alpha (6-9 Hz) band. However, their other findings could not be confirmed. Furthermore in this research, thresholds were established for distinguishing between healthy subjects and epilepsy patients. Together these findings demonstrate that this model could be used to provide significant additional information from rest-EEGs. This could ultimately lead to a better tool for identifying people with epilepsy leading to improved diagnostics and therapeutics.

# CONTENTS


1 Abstract 1

2 Introduction 3

3 The Kuramoto Model 4

4 Extended Kuramoto Model 8
- 4.1 Using $C_c$ as a measure for network-driven synchrony . . . 10
- 4.2 Using $r_g$ as a measure for node-driven synchrony . . . 12

5 Preparing rest-EEG for testing 13

6 Testing 15
- 6.1 Wilcoxon rank sum test/Mann-Whitney U test . . . 15
- 6.2 Friedman test . . . 16
- 6.3 Kruskal Wallis . . . 16
- 6.4 Leave-one-out method . . . 17

7 Results 18
- 7.1 Testing $C_c$ . . . 18
- 7.2 Testing $r_g$ . . . 18

8 Conclusion 20

9 Discussion 21

10 Bibliography 22

11 Appendix 25
- 11.1 Results . . . 25

# 2 INTRODUCTION

Recently a lot of research has been conducted to increase the understanding of the brain dynamics, particularly regarding abnormal behavior. In those researches graph theory is often used to explain phenomena like Parkinson and schizophrenia. Another neurological disorder that has recently gained a lot of attention is epilepsy, a disorder characterized by the tendency to have recurrent seizures. This disorder is one of the most common serious primary brain diseases, with a worldwide prevalence approaching 1% (Benjamin et al., 2011) [3]. So far this disorder has only been theoretically characterized as being associated with abnormal synchronization between brain regions. The International League Against Epilepsy (ILAE) defined an epileptic seizure as "a transient occurrence of signs and/or symptoms due to abnormal excessive or synchronous neuronal activity in the brain" [12].

Furthermore empirical data led to the idea that the cortical, frontal lobe is involved in absence seizures and primary generalized seizures. However, theoretical proof of this abnormal synchrony and which areas are involved could up to the point of the research conducted by Schmidt et al. (2014) not be given [25]. As a basis they used the Kuramoto model to model the brain and found markers in this model to distinguish between healthy subjects and epilepsy patients. According to them, with analysis based on this model, one can gain significant additional information from a routine clinical EEG (a rest-EEG), which eventually will lead to improved diagnostics and therapeutics of people with epilepsy. This could be an important breakthrough, since no epileptic seizures need to be induced to positively identify a person as having epilepsy. This inducing is time-consuming and not particularly nice for the patients. It also only leads to a positive diagnosis in a maximum of 60% of the cases, resulting in diagnostic uncertainty for many people. This leads to extra costs due to additional longer-term EEG monitoring, repeated hospital admissions, as well as unnecessary prescription of anti-epileptic drugs [26].

This paper will try to reproduce the findings of Schmidt et al. (2014) to be able to confirm their conclusion using another dataset.

# 3 THE KURAMOTO MODEL

As stated before the model used by Schmidt et al. is based on the Kuramoto model [25]. This is a standard model used to study synchronization phenomena. A reason for this is that this model is exactly solvable despite considering large sets of non-linearly coupled entities (Scholtes et al., 2009 [27]). For this purpose it is used as a purely phenomenological model, which allows analytical studies of synchronization phenomena in large scale networks. Recently, another model, the Wilson-Cowan model, was suggested to be a better model (Daffertshofer et al., 2011 [9]). This model is said to be better since it does not have the limit of weak coupling, which leads to neglecting the amplitude of the original model. However, the Kuramoto model is shown to already display behavior similar to epileptic seizures, so for this research a more detailed physiological model is not necessary [25].

The Kuramoto model describes the evolution of N identically coupled phase oscillators. Those N oscillators are coupled together uniformly with strength K through their phase $\theta$. The natural frequency of the $i^{th}$ oscillator is represented by $\omega_i$. Hereby is assumed that all these frequencies are drawn from a normal distribution function with mean $\Omega$ and standard deviation 1. This gives the following equation as defined by Kuramoto [14]:

$$\dot{\theta}_i = \omega_i + \frac{K}{N}\sum_{j=1}^{N}\sin(\theta_j - \theta_i) \tag{3.1}$$

Usually the collective behavior of the population oscillators is studied by calculating the order parameter r which measures the average amount of synchronization amongst oscillators. In figure 3.1 it can be seen that for a certain K-value a threshold is reached and $r$ becomes higher up to a coherence level of almost 1.

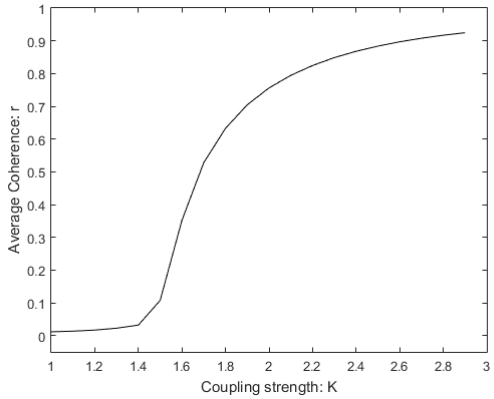


***Figure 3.1:*** *In this figure the average coherence r vs the coupling strength K is shown. It can be seen that for a certain K-value a threshold is reached and r becomes higher up to a coherence level of almost 1.*

To quantify this synchronization, r is defined in equation 3.2 with $\psi$ the average phase of the N phase-oscillators between 0 and $2\pi$:

$$re^{i\psi} = \frac{1}{N}\sum_{j=1}^{N} e^{i\theta_j} \tag{3.2}$$

Multiplying both sides by $e^{-\theta_i}$ equation 3.2 becomes:

$$re^{i(\psi-\theta_i)} = \frac{1}{N}\sum_{j=1}^{N} e^{i(\theta_j-\theta_i)} \tag{3.3}$$

Using Euler's formula equation 3.3 becomes:

$$r[\cos(\psi-\theta_i)+i\sin(\psi-\theta_i)] = \frac{1}{N}\sum_{j=1}^{N}[\cos(\theta_j-\theta_i)+i\sin(\theta_j-\theta_i)] \tag{3.4}$$

Equating the imaginary parts of equation 3.4 gives:

$$r\sin(\psi-\theta_i) = \frac{1}{N}\sum_{j=1}^{N}\sin(\theta_j-\theta_i) \tag{3.5}$$

Thus,equation 3.1 can be transformed in equation following the method of S. H. Strogatz (2000) [32]:

$$\dot{\theta}_i = \omega_i + rK\sin(\psi-\theta_i) \tag{3.6}$$

In this context a higher level of phase coherence is equivalent with a higher level of synchronization [36]. In figure 3.2 phase $\theta$ is plotted over time for all the different oscillators N (in this case $N = 10^3$).

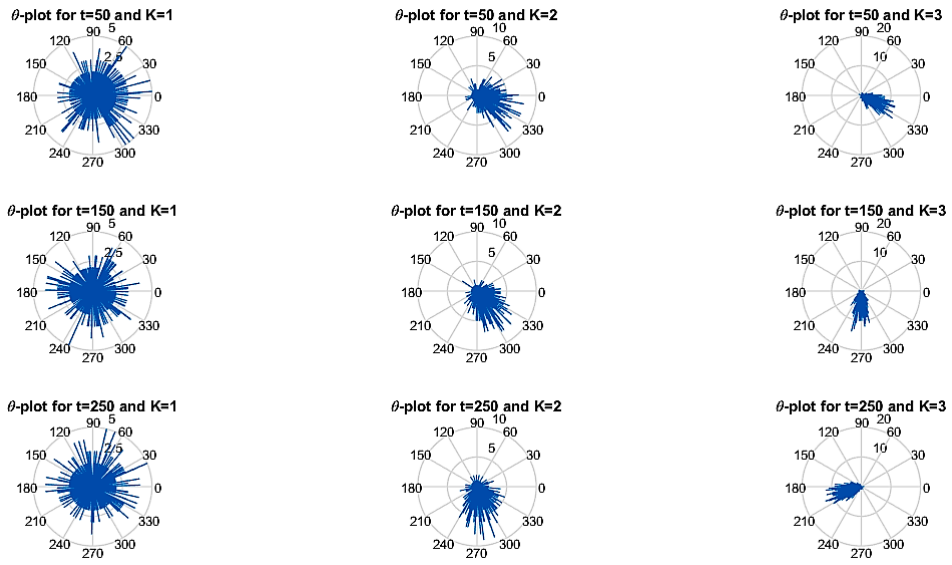


***Figure 3.2:*** *In this figure phase parameter $\theta$ is plotted over time (t-values of 50,150 and 250 ms are shown) for all the different oscillators N (in this case $N = 10^3$). This is done for the K-value of 1, 2 and 3. In this way it can be seen that when K becomes higher than a certain threshold all the phases of the different oscillators become phase-locked.*

In this way an illustration is given that higher than a certain K-value the phases $\theta$ become phase-locked. This shows that synchronization occurs when K becomes larger. Using these computations it can be concluded that a critical value for K, $K_c$, is the onset for synchronization. This is analogous to the transition between background and spike-wave activity seen in the onset of seizures. This synchronization phenomenon is called node-driven synchrony, since it can occur within a node. A node being here analogous to the coupling of those N oscillators. The theoretical value of this $K_c$ as proposed by Kuramoto is [10]:

$$K_c = \frac{2}{\pi g(0)} \tag{3.7}$$

The value g(0) comes from the probability distribution $g(\omega)$ from which $\omega_i$ are drawn. In this case the normal distribution is used with $\mu = 0$, since a prerequisite for choosing a distribution is that the distribution is symmetrical and that $g(\omega) = g(-\omega)$ [5]. Thus the probability distribution is

$$g(\omega) = \frac{1}{\sigma\sqrt{2\pi}} e^{-\left(\frac{\omega-\mu}{2\sigma^2}\right)^2} \quad \text{with } \mu = 0 \tag{3.8}$$

resulting in

$$g(0) = \frac{1}{\sigma\sqrt{2\pi}} \tag{3.9}$$

Using equation 3.9 in equation 3.7 gives

$$K_c = \frac{2}{\pi \frac{1}{\sigma\sqrt{2\pi}}} = \frac{2\sqrt{2\pi}}{\pi\frac{1}{\sigma}} = \frac{2\pi\sqrt{2}}{\pi\sqrt{\pi}\frac{1}{\sigma}} = \frac{2\sqrt{2}}{\sqrt{\pi}}\sigma \tag{3.10}$$

A simulation of this for different values of $\sigma$ is shown in figure 3.3.

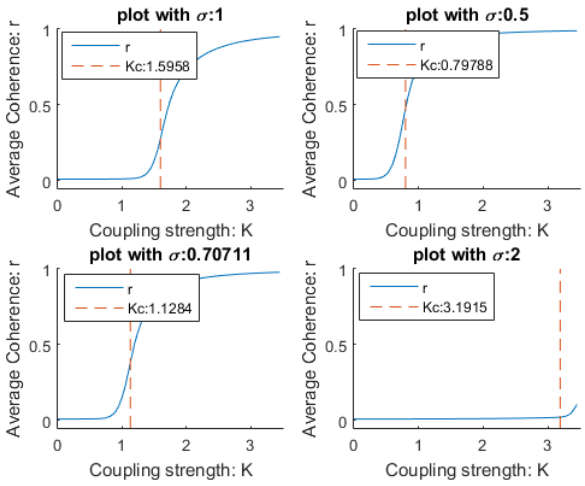


***Figure 3.3:*** *In this figure plots of K vs. r are shown again, but now for different values of σ. In this figure also the theoretical value of $K_c$ based on eq. 3.10 is shown. It can be seen that this theoretical value is approximately the onset for synchronization.*

However, since only a finite system can be simulated, the numerical onset for synchronization can only be approximated by the theoretical $K_c$ . That's why the proposal of Schmidt et al. (2014) to use a $K_c$ of $\frac{2}{\sqrt{\pi}}$, is used in the rest of the paper [25]. In figure 3.4 again a plot is shown of K vs. r with $\mu = 0$ and $\sigma = 1$ with also the theoretical and proposed value of $K_c$ shown. This shows that setting $K_c = \frac{2}{\sqrt{\pi}}$ is a logical choice.

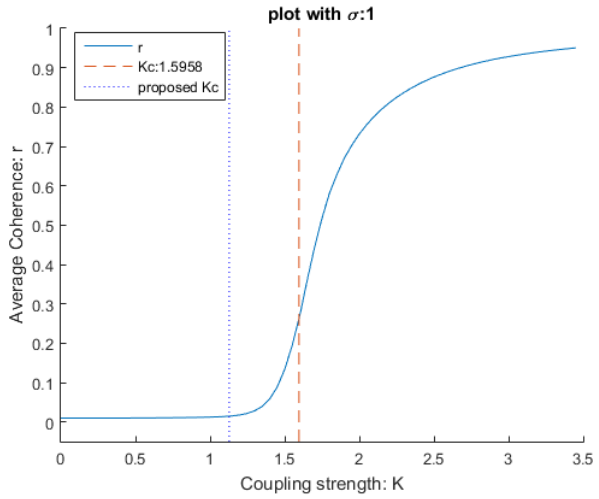


***Figure 3.4:*** *In this figure again K vs r is plotted. Now next to the theoretical value of $K_c$ also the proposed value of $K_c$ by Schmidt et al. (2014) [25] is shown. It can be seen that the proposed value is a good value to use, since no synchronization has occurred yet for smaller K-values, unlike for the theoretical value.*

To represent a collection of cortical columns N is set to use this model as a representation of the brain for modeling epilepsy. Together this network of N oscillators form node p, with a node representing a recording site. To be able to use the Kuramoto model, it is assumed that this network is all-to-all connected. However, since an EEG consists of multiple nodes, P such nodes were connected following the method of Barreto et al. (2008) [2]. Those P nodes thus all representing a Kuramoto model of N coupled oscillators.

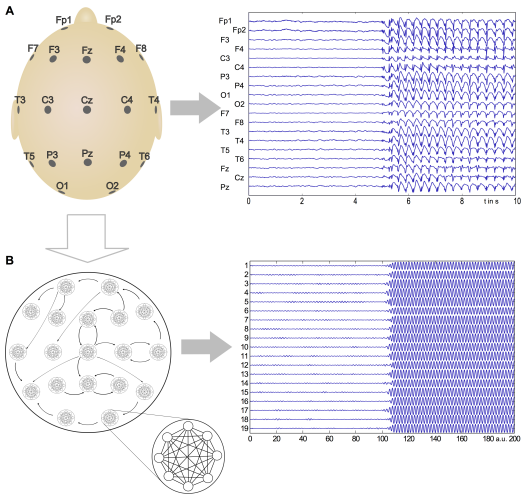


***Figure 4.1:*** *Comparison of recorded seizure with output Kuramoto model.* ***A:*** *EEG recording of epileptic seizure.* ***B:*** *Kuramoto model in which one node represents one recording site. The model within one node is an all-to-all connected network representing a collection of cortical columns [25].*

# 4 Extended Kuramoto Model

To connect P nodes (all nodes representing a Kuramoto model of N coupled oscillators) Barreto et al. introduced a $P \cdot P$ coupling matrix $\rho$ with entries $\rho_{p,q}$, representing the coupling strength from node q to node p. This describes the interaction between nodes p and q weighted by a global coupling parameter C. The equation for $\dot{\theta_i^p}$ then becomes (here super-or subscript p is introduced to point out that it resembles the variable for node p, the same holds for subscript q).

$$\dot{\theta_i^p} = \omega_i^p + \frac{K_p}{N}\sum_{j=1}^{N}\sin(\theta_j^p - \theta_i^p) + C\sum_{q=1}^{P}\frac{\rho_{p,q}}{N}\sum_{j=1}^{N}\sin(\theta_j^q - \theta_i^p) \tag{4.1}$$

Again following the same steps as in equation 3.2,3.3,3.4 and 3.5 equation 4.1 can be transformed in:

$$\dot{\theta_i^p} = \omega_i^p + r_p K_p \sin(\psi_p - \theta_i^p) + C\sum_{q=1}^{P} r_q \rho_{p,q}\sin(\psi_q - \theta_i^p) \tag{4.2}$$

with de order parameter $r_p$ for synchronicity here defined as:

$$r_p e^{i\psi_p} = \frac{1}{N}\sum_{n=1}^{N} e^{i\theta_n^p} \tag{4.3}$$

In this way the Kuramoto model is extended to represent EEG waves for all the recording sites. This is illustrated in figure 4.1. In this figure it can be seen that the Kuramoto model models epileptic EEG currents quite well. That is why this model was chosen. In figure 4.2 MatLab representations of this extended model are shown. For this the K-value is always chosen to be below the critical value of K to make sure that node-driven synchrony will not occur.

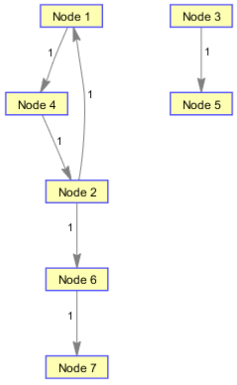


***(a)*** *Graph representation*

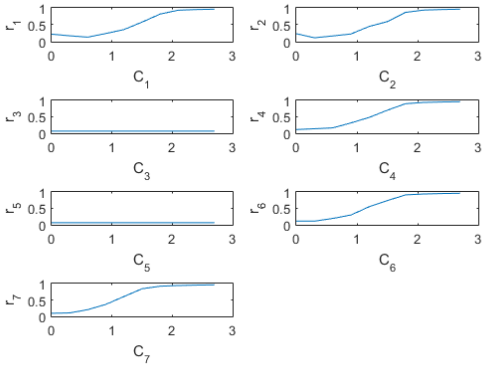


***(b)*** *Plots of C vs. $r_p$ for node p: 1-7*

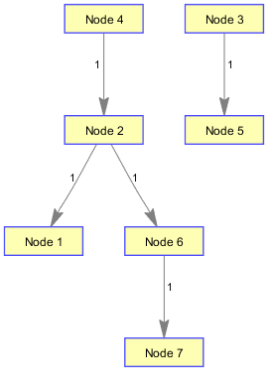


***(c)*** *Graph representation*

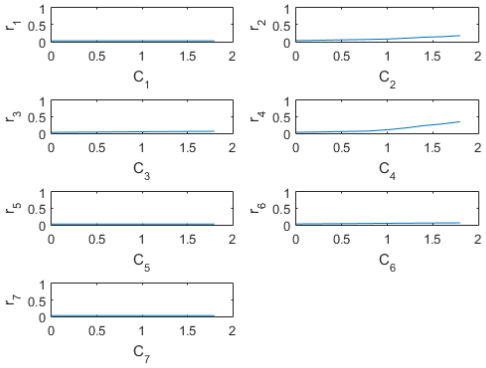


***(d)*** *Plots of C vs. $r_p$ for node p: 1-7*

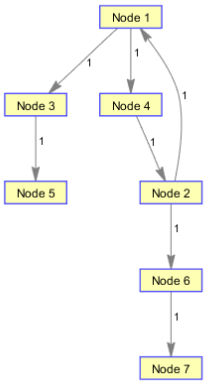


***(e)*** *Graph representation*

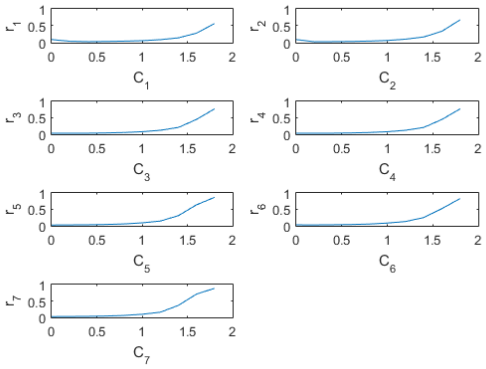


***(f)*** *Plots of C vs. $r_p$ for node p: 1-7*

***Figure 4.2:*** *Three different networks of seven nodes with their C (global coupling parameter) vs. $r_p$ (order parameter for synchronicity) plot. A $r_p$ of zero means no synchronicity and a $r_p$ of one means fully synchronized.*
***a:*** *It can be seen that in this network one cycle exists connecting node 1, 4 and 2 and node 6 and 7 connected to this cycle. All other nodes are disconnected.*
***b:*** *It can be seen that in this network only the nodes in the cycle and the connected nodes become synchronized ($r_p$ becomes high for a certain value of C for the nodes in the cycle).*
***c:*** *It can be seen that in this network no cycles exist.*
***d:*** *It can be seen that in this network all 7 nodes stay desynchronized ($r_p$ stays low).*
***e:*** *It can be seen that in this network one cycle exists connecting node 1, 4 and 2 and all other nodes are connected to this cycle.*
***f:*** *It can be seen that in this network all 7 nodes become synchronized ($r_p$ becomes high for a certain value of C).*
*$K_p$ is chosen lower than $K_c$ for all nodes to make sure no node-driven synchrony occurs.*

With this it can be seen that synchronization of the different nodes is influenced by the C-value. To illustrate this three different networks of seven nodes were created in MatLab: one with a cycle and two nodes connected to this and the other two disconnected (figure 4.2a), one with no cycles (figure 4.2c) and one with a cycle and all other nodes connected to the cycle (figure 4.2e). Comparing figure 4.2b with figure 4.2d it can be seen that the existence of cycles within the network plays a big role in this type of synchrony, since without the existence of cycles the curves of C vs. $r_p$ stay low for all nodes. However, if a cycle exists (in this case 1–>4–>2–>1) those curves shoot up at some critical value of C, called $C_c$. Also the nodes connected to this cycle become synchronized. This is clearly shown in figure 4.2f where all nodes are connected to the cycle in some way. This type of synchrony is called network-driven synchrony. With this type of synchrony it can occur that there is synchrony across the network while all the individual nodes are in desynchronized state. So the local coupling parameter $K_p$ is below the critical value $K_c$ and therefore all the individual nodes are not synchronized. This means that no node-driven synchrony occurs in this network.

## 4.1 Using $C_c$ as a measure for network-driven synchrony

As stated before, network-driven synchrony occurs when a certain value for C is reached, called $C_c$. To find this critical value one needs to find the value for which the equilibrium point of the system is degenerate [29]. To do this one first needs to create the Jacobian matrix of the system as defined in equation 4.2. This Jacobian matrix is defined as followed:

$$J = \left[ \frac{\partial \theta}{\partial r_1} \cdots \frac{\partial \theta}{\partial r_q} \right] = \begin{bmatrix} \frac{\partial \theta_1}{\partial r_1} & \cdots & \frac{\partial \theta_1}{\partial r_q} \\ \vdots & \ddots & \vdots \\ \frac{\partial \theta_q}{\partial r_1} & \cdots & \frac{\partial \theta_q}{\partial r_q} \end{bmatrix} \tag{4.4}$$

In this matrix the diagonal elements are the elements where one differentiates with respect to $r_p$ while considering node p. The other elements are also differentiated with respect to $r_p$ but now a node q is considered. Therefore those diagonal elements give a different solution than the other elements. Solving this Jacobian matrix for the extended Kuramoto model gives:

$$J = \begin{bmatrix} (K_1 + C \cdot \rho_{1,1}) \cdot \sin(\psi_1 - \theta_1) & \cdots & C \cdot \rho_{1,q} \cdot \sin(\psi_1 - \theta_q) \\ \vdots & \ddots & \vdots \\ C \cdot \rho_{q,1} \cdot \sin(\psi_q - \theta_1) & \cdots & (K_q + C \cdot \rho_{q,q}) \cdot \sin(\psi_q - \theta_q) \end{bmatrix} \tag{4.5}$$

Since we are looking for the point where network-driven synchrony starts, we want to make sure no node-driven synchrony occurs. Therefore on the diagonal elements the critical value for node-driven synchrony, $K_c$, is substracted from $K_p$, which will be defined as $K_{p,p}$. This leads to the following matrix:

$$J = \begin{bmatrix} (K_{1,1} + C \cdot \rho_{1,1}) \cdot \sin(\psi_1 - \theta_1) & \cdots & C \cdot \rho_{1,q} \cdot \sin(\psi_1 - \theta_q) \\ \vdots & \ddots & \vdots \\ C \cdot \rho_{q,1} \cdot \sin(\psi_q - \theta_1) & \cdots & (K_{q,q} + C \cdot \rho_{q,q}) \cdot \sin(\psi_q - \theta_q) \end{bmatrix} \tag{4.6}$$

Before this critical value occurs, there is no synchrony yet (since no node-driven synchrony, so the sinus elements in the matrix will be set to one to make sure that does not happen. This holds since without synchrony the order parameter $r_p = 0$. This gives the following Jacobian:

$$J = \begin{bmatrix} (K_{1,1} + C \cdot \rho_{1,1}) & \cdots & C \cdot \rho_{1,q} \\ \vdots & \ddots & \vdots \\ C \cdot \rho_{q,1} & \cdots & K_{p,p} + C \cdot \rho_{q,q} \end{bmatrix} \tag{4.7}$$

Now the final step in finding this critical C-value is solving $J = 0$, because that is the point where the system is degenerate. Since J is a matrix the solution can be found solving det(J)=0 This leads to the equation as proposed by Schmidt et al. (2014) [25]:

$$\det(C_c \rho + K) = 0 \tag{4.8}$$

with K being a $P \cdot P$-dimensional diagonal matrix with elements $K_{p,p} = K_p - K_c$ and $\rho$ being the connectivity matrix with elements $r_{p,q}$. Solving this equation gives the critical value $C_c$ for the onset of network-driven synchrony.

Testing this for a system with two nodes, one situation in which the nodes are connected and the other in which they are disconnected, gives $C_c = 0.3284, C_c$ non-existent, respectively. From this can be concluded that if no cycle exists, $C_c$ does not exist and no network-driven synchrony is possible. Changing the strength of all the bonds in the cycle in this two-node system from 1 to 0.5 gives $C_c = 0.6568$ and to 0.25 gives $C_c = 1.3135$. This leads to the conclusion that stronger bonds lead to a lower $C_c$-value. Even in a way that when the strength is halve the size, $C_c$ is twice as high. This can easily be explained by expanding $C_c \rho + K$:

$$\begin{bmatrix} 0 & \rho_{1,2} C_c \\ \rho_{2,1} C_c & 0 \end{bmatrix} + \begin{bmatrix} K_p - K_c & 0 \\ 0 & K_p - K_c \end{bmatrix} = \begin{bmatrix} K_p - K_c & \rho_{1,2} C_c \\ \rho_{2,1} C_c & K_p - K_c \end{bmatrix} \tag{4.9}$$

Solving equation 4.8 by using this expansion gives:

$$\begin{aligned} (K_p - K_c)^2 - \rho_{1,2}\rho_{2,1} \cdot C_c^2 &= 0 \\ (K_p - K_c)^2 &= \rho_{1,2}\rho_{2,1} \cdot C_c^2 \\ C_c^2 &= \frac{(K_p - K_c)^2}{\rho_{1,2}\rho_{2,1}} \\ C_c &= \sqrt{\frac{(K_p - K_c)^2}{\rho_{1,2}\rho_{2,1}}} \end{aligned} \tag{4.10}$$

From this equation it can clearly be seen that $C_c$ changes when the cycle changes and that when the cycle is broken, the denominator becomes zero and $C_c$ becomes non-existent. To test the influence of multiple cycles and cycle-size on $C_c$, $C_c$ was computed in a system with three nodes. The results can be found in table 4.1:

| **Cycle(s)** | **Other connection** | $C_c$ |
|---|---|---|
| 1-2-1 | no | 0.3284 |
| 1-2-1 | 2-3 | 0.3284 |
| 1-2-1 | 3-2 | 0.3284 |
| 1-3-2-1 | no | 0.3284 |
| 1-3-2-1 & 1-2-1 | no | 0.2479 |
| 1-2-1 & 2-3-2 | no | 0.2322 |

***Table 4.1:*** *Test of $C_c$ in a system with three nodes. In this test different systems with three nodes are created: one or more cycles and zero or one other connection. For those different systems the $C_c$-value is computed. It can be observed that the size of the cycle and whether there are other connections does not matter. However, it can be seen that the amount of cycles does matter ($C_c$ is lower) and that when the cycles are distinct that the $C_c$-value is even lower.*

From this table it can be concluded that the cycles in a system matter for the value of $C_c$. What can also be seen is that when there is only one cycle, the size of that cycle does not change the value of $C_c$. However, the amount of cycles does matter: more cycles gives a lower $C_c$, when those cycles are distinct even a lower value can be observed. Those are interesting observations, since according to Schmidt et al. (2014) the $C_c$-value is significantly lower for epileptic patients [25]. This would mean that those patients probably have more and stronger cycles than healthy subjects, explaining the lower $C_c$-value. To test their statement statistical analysis is performed to compare this $C_c$-value for epileptic patients with that of healthy subjects.

## 4.2 Using $r_g$ as a measure for node-driven synchrony

In the previous section $K_p$ was set at a smaller value than $K_c$ making sure that node-driven synchrony did not occur. However, it was also stated that if no cycles exist, no $C_c$-value could be found and no network-driven synchrony is possible. Also network-driven synchrony only occurred for a C-value larger than $C_c$. In those cases it could still be possible for synchrony across the network to occur caused by node-driven synchrony. To test this, C is set at a very low value ($< C_c$), making sure no network-driven synchrony occurs. As a measure for node-driven synchrony the order parameter $r_g$ is used, which is defined as the average of $r_p$ (see equation 4.3) over all P nodes:

$$r_g = \left| \frac{1}{P} \sum_{p=1}^{P} r_p e^{i\psi_p} \right| \tag{4.11}$$

This is a suitable way for defining $r_g$, since $r_p$ is the measure of phase coherence within one node. A $r_p$ close to zero means hardly any synchrony within the node and $r_p$ close to one means a lot of synchrony within the node. So a higher $r_g$ means that more nodes in the network are synchronized. To test the influence of one node being synchronized on the network as a whole, the K-value for that node is set higher than $K_c$ (meaning that this node will automatically synchronize) and the other K-values lower.

# 5 PREPARING REST-EEG FOR TESTING

However, before the parameters $r_g$ and $C_c$ can be used for analysis of real data, it is necessary to create the connectivity matrix $\rho$, which was introduced in the previous section. This connectivity matrix is extracted from a rest-EEG. Since in this research it is tried to reproduce the findings of Schmidt et al. (2014) their way of extracting data is used [25]. Therefore a 20 second segment of background activity (meaning eyes-closed) of a recorded rest-EEG needs to be extracted. To achieve this, appropriate rest-EEGs were selected and put in MatLab. With the help of MatLab a 20 second segment with the annotation along the lines of 'eyes closed' was selected. Then this segment had to be bandpass filtered between 1-70 Hz to exclude noise. For this the default bandpass filter in MatLab was used. Afterwards it was notch-filtered between 48-52 Hz to exclude interference from wires, light fluorescents and other equipments which are captured by the electrodes and acquisition system (Correa et al., 2011 [8]). The suggestion of using a notch filter stems from the work of Sameni (2012) [24]. However, for the implementation in MatLab the IIR notch filter was used, since according to Nehorai (1985) this gives better results when implemented by filtering out all that is desired [21].

This data is then divided into 5 frequency bands 5.1 based on the work of Shackman et al. (2010) [30]. However, another subdivision in the was made alpha band, since recent work from Chowdhury et al. (2014) found significant differences in rest-EEG data of the different alpha bands between epileptic patients and healthy subjects [7]. This led to this division:

| **Frequency band** | **Range** |
|---|---|
| delta | 1-3 Hz |
| theta | 3-6 Hz |
| low alpha | 6-9 Hz |
| high alpha | 10-14 Hz |
| beta | 15-30 Hz |
| gamma | 30-70 Hz |

***Table 5.1:*** *Division of rest-EEG into the different frequency bands used for this research.*

To look at the interdependencies between the different nodes within a frequency band, time-lagged cross-correlation is used. The method used is a linear method proposed by Bialonski et al. (2013) [4]. They proposed two methods. For this purpose the method taking time-lagging into account is necessary, since there might be time lags due to propagation of electrical activity along anatomical pathways during the seizure. It is possible to use a linear method, since according to research conducted by Stam et al. (2009) a resting-EEG is predominantly linear [31]. This gives the following equation for the coupling matrix $\rho$:

$$\rho_{p,q} = \max_{\tau} \left| \frac{\xi(x_p, x_q)(\tau)}{\sqrt{\xi(x_p, x_p)(0)\xi(x_q, x_q)(0)}} \right| \quad \text{where} \quad \xi(x_p, x_q)(\tau) = \begin{cases} \sum_{t=1}^{T-\tau} x_p(t+\tau)x_q(t) & \text{if } \tau \geq 0 \\ \sum_{t=1-\tau}^{T} x_p(t+\tau)x_q(t) & \text{if } \tau < 0 \end{cases} \tag{5.1}$$

Since this data is of finite length there could be autocorrelation effects included in this coupling matrix. Therefore 99 surrogate datasets are created from the original EEG data via the iterative amplitude-adjusted Fourier transform (IAAFT). This is proven to be an effective method by Maiwald et al. (2008) [17] and Schreiber et al. (1996) [28]. Coupling matrices are also created from these surrogate data. Comparing these with the actual coupling matrix, connections $\rho_{p,q}$ are rejected when they do not exceed the 95% level of significance. Following the method of Schmidt et al. then a directional matrix is created by setting $\rho_{p,q} = 0$ if $\tau_{p,q} \leq 0$ and $\rho_{q,p} = 0$ if $\tau_{p,q} \geq 0$. With this the zero time-lag connections are also removed. Furthermore spurious connections are removed, meaning direct connections between nodes are removed when stronger indirect connections via one or two other nodes exist.

All of the steps above give the functional connectivity matrix $\rho$, which can be used for further testing. An illustration of this procedure can be seen in figure 5.1.

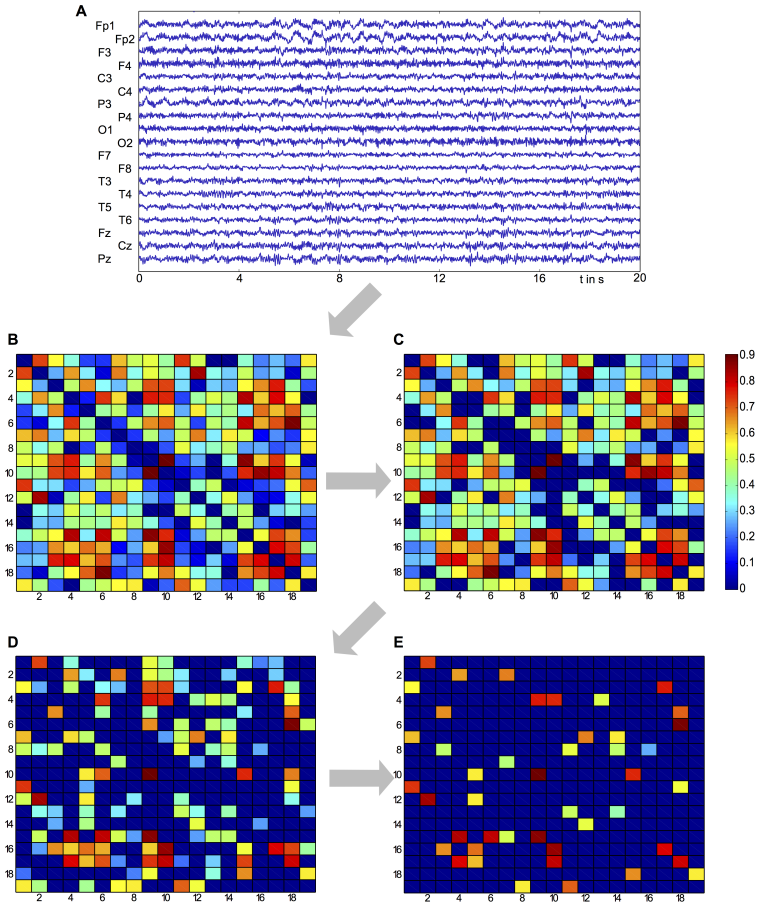


***Figure 5.1:*** *Illustration of the procedure to derive the functional network structure.* ***A:*** *An artefact-free 20s resting-state segment of EEG from each subject is extracted.* ***B:*** *Applying the time-lagged cross-correlation to all combinations of channel pairs yields a bidirectional connectivity matrix.* ***C:*** *Connections are removed if they are not significantly different from surrogate data (95% level of significance).* ***D:*** *Using the time-lags, a unidirectional connectivity matrix can be inferred.* ***E:*** *Setting to zero all connections that can be explained by stronger, indirect connections removes spurious connections. [25]*

# 6 TESTING

Now the connectivity matrix can be computed based on real rest EEG-data. For this 43 patients were selected (18 male/25 female) above the age of 10, all categorized as having primary generalized epilepsy (sample A). About half of the patients use anti-epileptica. This data was compared to a control-group of 41 subjects (19 male/22 female) also above the age of 10 (sample B). After computation of the connectivity matrices for all frequency bands for all subjects, $C_c$ and $r_g$ can be computed for all the connectivity matrices. For $r_g$ per frequency band 19 results were computed, one for every node. This is summarized in table 6.1.

| **Frequency band** | $C_c$**-results** | **total** $C_c$**-results** | $r_g$**-results** | **total** $r_g$**-results** |
|---|---|---|---|---|
| delta | 1 per subject | A:43, B:41 | 19 per subject | A:19·43, B:19·41 |
| theta | 1 per subject | A:43, B:41 | 19 per subject | A:19·43, B:19·41 |
| low alpha | 1 per subject | A:43, B:41 | 19 per subject | A:19·43, B:19·41 |
| high alpha | 1 per subject | A:43, B:41 | 19 per subject | A:19·43, B:19·41 |
| beta | 1 per subject | A:43, B:41 | 19 per subject | A:19·43, B:19·41 |
| gamma | 1 per subject | A:43, B:41 | 19 per subject | A:19·43, B:19·41 |

***Table 6.1:*** *Summary of all the different calculations performed used for statistical testing. The value 19 stems from all the different nodes used. A stands for sample A: patients with primary generalized epilepsy and B stands for sample B: control-group.*

On all these results statistical tests need to be performed to test the results of Schmidt et al. (2014), who stated that there were significant differences between sample A and sample B [25].

First of all the Kolmogorov-Smirnov test was performed on all these results to test whether the underlying distribution of both sample A and sample B was normal. This test returns a test decision for the null hypothesis that the data in vector x comes from a standard normal distribution, against the alternative that it does not come from such a distribution. The result h is 1 if the test rejects the null hypothesis at the 5% significance level, or 0 otherwise. For all data-vectors this test returned a 1, so we cannot assume that the underlying distributions are normal. This result is important, since now no test for comparing the two samples can be used which assumes an underlying normal distribution, like the t-test. However, there are a couple of statistical tests which can be used that do not make this assumptions. Schmidt et al. (2014) used the Wilcoxon rank sum test [25].

However, other commonly used possibilities are the Mann-Whitney U test, the Kruskal Wallis and the Friedman test. The latter was used in the work of Schmidt et al. (2016) [26]. These four possible tests are compared and contrasted to eventually be able to choose a suitable test for our data.

## 6.1 WILCOXON RANK SUM TEST/MANN-WHITNEY U TEST

The Mann-Whitney U test is basically the same as the Wilcoxon rank sum test. In most of the literature they are used interchangeably. The Wilcoxon rank sum test is the test that was originally used in the work of Schmidt et al. (2014) [25]. In this test a vector is created

containing all data, so both of sample A and sample B. The data is then categorized in ascending order and each value is given a rank according to the position which it is in. If two or more data-points have the same value they will all get the average rank. Then the sum of the ranks is calculated for both samples. Afterwards the hypothesis $H_0$: A = B is tested versus $H_1$: A < B (in case of $C_c$-values) or $H_1$: A > B (in case of $r_g$-values).

This test, like any non-parametric test, does not depend on assumptions on the distribution. So one can also use it when, as in this case, the normality of the distribution cannot be confirmed. Another advantage of this test is that it is less sensitive to outliers. When samples are paired the Wilcoxon signed rank test is used, which is a slightly different test, but this is not the case here. So this looks like quite an appropriate test. However, it is shown that this test can give wrongfully significant results when the two samples are drawn from two populations with the same average but with different variances. This could then lead to a rejection of the null-hypothesis, while this is actually true [20].

## 6.2 Friedman test

The Friedman test is mostly used for three or more correlated samples. Since our data is not correlated, this measurement is not appropriate to use. For completeness a short explanation of the test is still given. Per subject the different samples are ranked (highest score, highest ranking). Then the sum ($T_g$) and the mean of those rankings are calculated. Eventually this will lead to formula for chi-squared, which is the statistic used by this test:

$$\chi^2 = \frac{\sum\left(\frac{(T_g)^2}{n}\right) - \frac{(T_{all})^2}{nk}}{\frac{k(k+1)}{12}} \quad \text{with n = nr. of subjects, k = measurements per subject and df = k-1} \tag{6.1}$$

With this statistic the null-hypothesis can be tested [15].

## 6.3 Kruskal Wallis

The Kruskal Wallis is in essence the same as the Wilcoxon rank sum test. It also ranks all the data according to the position of the data in an ascending vector of all values. The main difference is that this test is mostly used for three or more samples. Next to the sums of ranks takes this test also the averages of each group into account. Therefore this might be a more accurate measurement than the Wilcoxon rank sum test, also when only considering two samples. However, this test only checks whether the distributions are different and not if one is greater/smaller than the other. The test statistic used in this test is H, which is formulated as followed:

$$H = \frac{\sum\left(\frac{(T_g)^2}{n_g}\right) - \frac{(T_{all})^2}{N}}{\frac{N(N+1)}{12}} \qquad \text{with} \tag{6.2}$$

$T_g$ = sum of ranks of group,
$T_{all}$ = sum of ranks total,
$n_g$ = number of samples of group,
N = total number of samples.

This statistic is a close approximation of the chi-squared distribution when each of the k samples has a sample size larger than 5 with df = k-1. In this way the null-hypothesis can be tested [16].

The best test seems to be Kruskal Wallis. However, we want to find out if the data confirms our hypotheses. This means confirming that the $C_c$ of epileptic patients is smaller than the $C_c$ of the control group and that the $r_g$ of epileptic patients is greater than the $r_g$ of the control group. Therefore we want to perform left-tailed tests and right-tailed tests respectively. So for this purpose the Wilcoxon rank sum test is used.

## 6.4 Leave-one-out method

Another test used to take a more detailed look to the specificity and sensitivity of the different markers is the leave-one-out method.This method was proposed by Schmidt et al. (2016) as a good method for testing [26]. This test pools all the data (both of the epilepsy patients and the control group) and successively leaves one subject out. The remaining data is used as the training set. With this method thresholds are determined to give the highest sensitivity for 100% specificity and the highest specificity for 100% sensitivity. Afterwards these thresholds are used to classify the test subject: if the value is on the epilepsy side of both thresholds (in the case of $C_c$ below and in the case of $r_g$ above), then it is classified as epilepsy. If the value is on the control side of both thresholds, the value is classified as control. If the value lies between the two thresholds, the value is classified as uncertain. An illustration of this method is shown in figure 6.1.

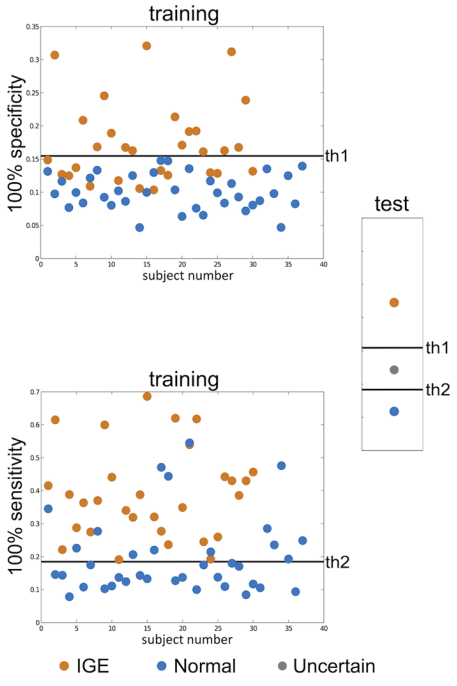


***Figure 6.1:*** *The leave-one-out method*
*This test pools all the data (both of the epilepsy patients and the control group) and successively leaves one subject out. The remaining data is used as the training set. With this method thresholds are determined to give the highest sensitivity for 100% specificity and the highest specificity for 100% sensitivity. Afterwards these thresholds are used to classify the test subject: if the value is on the epilepsy side of both thresholds, then it is classified as epilepsy. If the value is on the control side of both thresholds, the value is classified as control. If the value lies between the two thresholds, the value is classified as uncertain. [26].*

# 7 Results

## 7.1 Testing $C_c$

As stated before a left-tailed Wilcoxon rank sum test was performed. This gave the following results:

| **Frequency band** | **p-value** |
|---|---|
| delta | 0.3737 |
| theta | 0.5919 |
| low alpha | **0.0761** |
| high alpha | 0.3866 |
| beta | 0.2689 |
| gamma | 0.3496 |

***Table 7.1:*** *In this table the found p-values for the different frequency bands are shown. These value were computed using a left-tailed Wilcoxon rank sum test for comparison of the $C_c$-values of the epileptic patients and the control-group. The value printed in bold is a significant p-value when $\alpha$ is set to 0.1.*

As can be seen in table 7.1 the only band that gives significant results is the low alpha band. This band gives a significant value when $\alpha$ is set to 0.1.

Using the leave-one-out method for this biomarker gives the following results, see table 7.2. However, none of the bands give significant results.

| **Fr. band** | **thr. spec.** | **thr. sens.** | **epi class. as epi** | **contr class. as contr** | **spec.** | **sens.** |
|---|---|---|---|---|---|---|
| delta | 0.6233 | 0.6233 | 43/43 | 1/41 | 2.4% | 100% |
| theta | 0.8809 | 0.7719 | 42/43 | 1/41 | 2.4% | 97.7% |
| low alpha | 0.2455 | 0.2192 | 0/43 | 40/41 | 97.6% | 0% |
| high alpha | 0.2333 | 0.1745 | 0/43 | 39/41 | 95.1% | 0% |
| beta | 2.0169 | 2.0169 | 21/43 | 14/41 | 34.1% | 48.8% |
| gamma | 0.7083 | 0.8330 | 3/43 | 41/41 | 100% | 7.0% |

***Table 7.2:*** *Leave-one-out method applied on the $C_c$-values for all the different frequency bands.*

## 7.2 Testing $r_g$

As stated before a right-tailed Wilcoxon rank sum test was performed for the testing of the biomarker $r_g$. This gave the following significant results (p-value less than 0.05):

- The p-value for node F3 of the beta band is 0.0272.
- The p-value for node C4 of the beta band is 0.0346.
- The p-value for node T5 of the low alpha band is 0.0112.
- The p-value for node Cz of the gamma band is 0.0078.
- The p-value for node Pz of the high alpha band is 0.0375.

For all the results, see table 11.1 in Appendix 11.1, with those significant values printed in bold.

Also for this biomarker the leave-one-out method was performed, this time giving some interesting results:

- Node P4 of the delta band:
  - 42/43 epilepsy patients and 19/41 controls were classified correctly.
  - 0/43 of the epilepsy patients and 2/41 controls were classified as undefined.
  - 1/43 of the epilepsy patients and 19/41 controls were wrongly classified.
- Node Fz of the delta band:
  - 21/43 epilepsy patients and 40/41 controls were classified correctly.
  - 0/43 epilepsy patients and 0/41 controls were classified as undefined.
  - 22/43 epilepsy patients and 1/41 controls were wrongly classified.
- Node P3 of the low alpha band:
  - 42/43 epilepsy patients and 20/41 controls were classified correctly.
  - 1/43 epilepsy patients and 2/41 controls were classified as undefined.
  - 1/43 epilepsy patients and 20/41 controls were wrongly classified.
- Node T5 of the high alpha band:
  - 22/43 epilepsy patients and 40/41 controls were classified correctly.
  - 0/43 epilepsy patients and 1/41 controls were classified as undefined.
  - 21/43 epilepsy patients and 0/41 controls were wrongly classified.
- Node F7 of the gamma band:
  - 21/43 epilepsy patients and 40/41 controls were classified correctly.
  - 0/43 epilepsy patients and 0/41 controls were classified as undefined.
  - 22/43 epilepsy patients and 1/41 controls were wrongly classified.

The complete table with all results (notable results marked in bold) and also the values for th1 and th2 can be found in Appendix 11.1 table 11.2.

# 8 Conclusion

The Kuramoto model and then specifically the extended Kuramoto model seems to be a good tool to model brain waves found in an EEG. Also the theoretical model shows the effect of the biomarkers $C_c$ and $r_g$ on synchronicity very well. This shows that more and stronger cycles lead to a lower $C_c$-value, causing synchronicity across the network to occur more easily. The $r_g$-value is higher when the node that is set to synchronize has a higher effect on the synchronicity across the network as a whole. Therefore, theoretically, those two biomarkers seem to be appropriate for distinguishing between epilepsy patients and healthy subjects. Since it is believed that epilepsy is caused by abnormal or excessive synchronous activity in the brain.

However, when testing those biomarkers on real resting EEG data hardly any significant results were found. For the $C_c$-value only the low alpha band gave promising results for a 90% significance level. But then using the leave-one-out method, no interesting results were found. The biomarker $r_g$ looks a little more promising: node F3 and C4 of the beta band, node T5 of the low alpha band, node Pz of the high alpha band and node Cz of the gamma band all gave significant results for a significance level of 95%.

Especially the leave-one-out method for this biomarker gave some promising results for diagnostic purposes, since it either classified almost all controls correctly and about 50% of the epilepsy patients (1) or the other way around (2). Those markers were for option 1:

- Node Fz of the delta band: 97.6 % specificity and 48.8% sensitivity.
- Node T5 of the high alpha band: 97.6 % specificity and 51.2 % sensitivity.
- Node F7 of the gamma band: 97.6 % specificity and 48.8% sensitivity.

And for option 2:

- Node P4 of the delta band: 46.3% specificity and 97.7% sensitivity.
- Node P3 of the low alpha band: 48.8% specificity and 97.7% sensitivity.

So the method proposed by Schmidt et al. (2014) seems to be a good method theoretically. However, the results they found could not be reproduced, when testing the method on a new set of data. Only the biomarker $C_c$ for the low-alpha band also gave significant results for this new dataset.

# 9 Discussion

There were some statistically significant results found using the Wilcoxon rank sum test. However, looking at it more critically those results for the biomarker $r_g$ could just be random, since some p-values were that high that they would have given a significant results when the hypothesis was formulated exactly the other way around (using a left-tailed Wilcoxon rank sum test instead of a right-tailed). Also comparing these results with the results found by Schmidt et al. (2014) [25] and Schmidt et al. (2016) [26] completely different results were found again. This supports the suspicion that those results were all just found randomly and that every dataset used for this analysis gives again another result.

Even though hardly any results could be found, using the Kuramoto model as a diagnostic tool for epilepsy could work. Theoretically it still seems a good model and more research should be conducted to see if this model can or cannot be used in a clinical setting.

One big advantage of this model is that a rest-EEG can be used, so no provocation of epileptic seizures is needed. This would be an improvement, since this induction is time-consuming, costly and not particularly nice for the patients. Furthermore anyone can analyze this rest-EEG, since only a piece annotated with 'eyes closed' has to be selected and then the data can be put in the model. So at first no expert in analyzing EEGs is needed.

However, the results found in this research do not look promising, since there could be multiple other explanations given for not finding significant differences. First of all, for this research data of people diagnosed with having idiopathic generalized epilepsy were selected and people who came to the hospital for whatever reason and then eventually classified as normal after having had an EEG. This could have led to wrongly used data, since the people classified as normal could still have epilepsy but with it not being detected (yet). Furthermore, the epilepsy patients were all classified by an expert as having idiopathic generalized epilepsy, however it could be that some were classified incorrectly and actually had another type of epilepsy.

Also some of the epileptic patients used medicines as treatment for their epilepsy. It could be that those drugs influenced the network structure in such a way that no significant differences could be found. To test this a comparison should be made between the patients with and without medication for epilepsy to test whether significant differences could be found between them.

So to really be able to use the Kuramoto model as a diagnostic tool for epilepsy further testing needs to be done on a very large scale. There could definitely still be a future in using this model, especially when looking at the results of the biomarker $r_g$ of the leave-one-out method. Based on these results, it could still be possible to develop a nice diagnostic tool for testing on epilepsy.

# 10 BIBLIOGRAPHY


[1] Acebrón J.A., Bonilla L.L., Vicente C.J.P., Ritort F., Spigler R. (2005). *The Kuramoto model: a simple paradigm for synchronization phenomena.* Reviews of modern physics 77:138-185.

[2] Barreto E., Hunt B., Ott E., So P. (2008). *Synchronization in networks of networks: The onset of coherent collective behavior in systems of interacting populations of heterogeneous oscillators.* Phys Rev E 77(3 Pt 2).

[3] Benjamin O., Fitzgerald T.H.B., Ashwin P., Tsaneva-Atanasova K., Chowdhury F.A., Richardson M.P., Terry J.R. (2012). *A phenomenological model of seizure initiation suggests network structure may explain seizure frequency in idiopathic generalised epilepsy.* Journal of Mathematical Neuroscience 2:1.

[4] Bialonski S., Lehnertz K. (2013). *Assortative mixing in functional brain networks during epileptic seizures.* Chaos 23

[5] Botcharova M., Farmer S.F., Berthouze L. (2014). *Markers of cirticaltity in phase synchronization.* Frontiers in Systems Neuroscience 8: 22-45.

[6] Bullmore E. Sporns O. (2009).*Complex brain networks: graph theoretical analysis of structural and functional systems.* Nat Rev Neurosci 10: 186-189.

[7] Chowdhurry F.A., Woldman W., FitzGerald T.H., Elwes R.D., Nashef L., Terry J.R., et al.(2014). *Revealing a brain network endophenotype in families with endophenotype in families with idiopathic generalised epilepsy.* PloS One 9(10).

[8] Correa M.A.G., Leber E.L. (2011). *Noise Removal from EEG Signals in Polisomnographic Records Applying Adaptive Filters in Cascade,* Adaptive Filtering Application, Dr Lino Garcia (Ed.). InTech.

[9] Daffertshofer A., van Wijk B.C.M. (2011). *On the influence of amplitude on the connectivity between phases.* Front Neuroinf 5(6).

[10] Daniels B.C. (2005). *Synchronization of Globally Coupled Nonlinear Oscillators: the Rich Behavior of the Kuramoto Model.* Ohio Wesleyan Physics Dept. 7(2).

[11] Dörfler F., Bullo F. (2011). *On the Critical Coupling for Kuramoto Oscillators.* SIAM Journal on Applied Dynamical Systems 10(3):1070-1099.

[12] Fisher R.S., van Emde-Boas W., Blume W. Elger C., Genton P, et al. (2005). *Epileptic seizures and epilepsy: definitions proposed by the international league against epilepsy (ILAE) and the international bureau for epilepsy (IBE).* Epilepsia 46: 470-471.

[13] Hanley J.A., McNeil B.J. (1982). *The Meaning and Use of the Area under a Receiver Operating Characteristic (ROC) curve.* Radiology 143: 29-36.

[14] Kuramoto Y. (1984). *Chemical oscillations, waves and turbulence.* Springer, New York.

[15] Lowry R. (2015) *The Friedman Test for 3 or More Correlated Samples*. VassarStats.

[16] Lowry R. (2015). *The Kruskal-Wallis Test for 3 or More Independent Samples*. VassarStats.

[17] Maiwald T., Mammen E., Nandi S., Timmer J. (2008). *Surrogate Data - A Qualitative and Quantitative Analysis*. Mathematical Methods in Signal Processing and Digital Image Analysis, Understanding Complex Systems. 41-74.

[18] Montbrió E., Kurths J., Blasius B. (2004). *Synchronization of two interacting populations of oscillators*. Phys Rev E 70(5).

[19] Mormann F., Lehnertz K., David P., Elger C.E. (2000). *Mean phase coherence as a measure for phase synchronization and its application to the EEG of epilepsy patients*. Physica D 144: 358-369.

[20] Nachar N. (2008). *The Mann-Whitney U: A Test for Assessing Whether Two Independent Samples Come from the Same Distribution*. Tutorials in Quantitative Methods for Psychology 4(1): 13-20.

[21] Nehorai A. (1985). *A Minimal Parameter Adaptive Notch Filter With Constrained Poles and Zeros*. IEEE Transactions on Acoustics, Speech, and Signal Processing 33(4).

[22] Petkov G., Goodfellow M., Richardson M.P., Terry J.R. (2014). *A critical role for network structure in seizure onset: a computational modeling approach*. Frontiers in Neurology 5(261).

[23] Rodrigues F.A., Peron T.K.DM., Ji P., Kurths J. (2016). *The Kuramoto model in complex networks*. Physics Reports 610. 1-98.

[24] Sameni R. (2012). *A Linear Kalman Notch Filter for Power-Line Interference Cancellation*. Proceedings of the 16th CSI International Symposium on Artificial Intelligence and Signal Processing (AISP '12). 604-610.

[25] Schmidt H., Petkov G., Richardson M.P., Terry J.R. (2014). *Dynamics on Networks: The Role of Local Dynamics and Global Networks on the Emergence of Hypersynchronous Neural Activity*. PLoS Comput Biol 10(11).

[26] Schmidt H., Woldman W., Goodfellow M., Chowdhury F.A., Koutroumanidis M., Jewell S., Richardson M.P., Terry J.H. (2016). *A computational biomarker of idiopathic generalized epilepsy from resting state EEG* Epilepsia 57(10): 200-204.

[27] Scholtes I., Botev J., Esch M., Sturm P. (2009). *Epidemic Self-Synchronization in Complex Networks*. Systemsoftware and Distributed Systems.

[28] Schreiber T., Schmitz A. (1996). *Improved Surrogate Data for Nonlinearity Tests*. Physical Review 77(4).

[29] Schumaker M.F. (2010). *8.1 Bifurcations of equilibria*. Washington State University.

[30] Shackman A.J., McBenamin B.W., Maxwell J.S., Greischar L.L., Davidson R.J. (2010). *Identifying robust and sensitive frequency bands for interrogating neural oscillations.* NeuroImage 51: 1319-1333.

[31] Stam C.J., Pijn J.P.M., Suffczynski P., da Silva F.H.L. (1999). *Dynamics of the human alpha rhythm: evidence for non-linearity?* Clinical Neurophysiolog 110(10):1801-1813.

[32] Strogatz S.H. (2000). *From Kuramoto to Crawford: exploring the onset of synchronization in populations of coupled oscillators.* Physica D 143:1-20

[33] Terry J.R., Benjamin O., Richardson M.P. (2012). *Seizure generation: The role of nodes and networks.* Epilepsia 53(9):166-169.

[34] Varela F., Lachaux J.P., Rodriguez E., Martinerie J. (2001) *The brainweb: Phase synchronization and large-scale integration.* Nat Rev Neurosci 2: 229-239.

[35] Wilcoxon F. *Individual Comparisons by Ranking Methods.* Biometrics Bulletin 1(6): 80-83.

[36] Yan B., Li P. (2013). *The emergence of abnormal hypersynchronization in the anatomical structural network of human brain.* NeuroImage 65:34-51.

# 11 Appendix

## 11.1 Results

| Node | p delta | p theta | p l. alpha | p h. alpha | p beta | p gamma |
|---|---|---|---|---|---|---|
| Fp2 | 0.9723 | 0.9734 | 0.6564 | 0.1581 | 0.2077 | 0.4857 |
| Fp1 | 0.7403 | 0.9815 | 0.5534 | 0.6432 | 0.4360 | 0.3177 |
| F4 | 0.8122 | 0.9890 | 0.3771 | 0.6855 | 0.7135 | 0.7166 |
| F3 | 0.8644 | 0.7974 | 0.3976 | 0.3737 | **0.0272** | 0.2539 |
| C4 | 0.6058 | 0.9654 | 0.5955 | 0.4537 | **0.0346** | 0.2988 |
| C3 | 0.6727 | 0.3873 | 0.9252 | 0.6161 | 0.9802 | 0.6398 |
| P4 | 0.7043 | 04964 | 0.3050 | 0.9483 | 0.4466 | 0.1830 |
| P3 | 0.4360 | 0.4964 | 0.5710 | 0.6531 | 0.4857 | 0.6093 |
| O2 | 0.5885 | 0.7166 | 0.3403 | 0.4011 | 0.9012 | 0.2370 |
| O1 | 0.3669 | 0.6950 | 0.3370 | 0.7432 | 0.4786 | 0.7074 |
| F8 | 0.5920 | 0.5498 | 0.1927 | 0.9879 | 0.5428 | 0.7766 |
| F7 | 0.4929 | 0.3081 | 0.1170 | 0.4715 | 0.6662 | 0.3436 |
| T4 | 0.3568 | 0.9871 | 0.3830 | 0.5710 | 0.1317 | 0.2288 |
| T3 | 0.9625 | 0.3703 | 0.3635 | 0.8882 | 0.1084 | 0.6630 |
| T6 | 0.2001 | 0.8097 | 0.7135 | 0.6297 | 0.4045 | 0.2001 |
| T5 | 0.5071 | 0.8800 | **0.0112** | 0.5498 | 0.5071 | 0.9434 |
| Fz | 0.7074 | 0.6823 | 0.8504 | 0.6093 | 0.9717 | 0.1496 |
| Cz | 0.9336 | 0.4360 | 0.9633 | 0.4893 | 0.2370 | **0.0078** |
| Pz | 0.5605 | 0.1395 | 0.6887 | **0.0375** | 0.9834 | 0.5000 |

***Table 11.1:*** *Found p-value for different frequency bands and different nodes for comparing $r_g$ epilepsy patients and control-group using the right-tailed Wilcoxon rank sum test.*

| Node | fr. band | thr. spec. | thr. sens. | epi class. as epi | contr class. as contr | spec. | sens. |
|---|---|---|---|---|---|---|---|
| Fp2 | delta | 0.0704 | 0.0811 | 41/43 | 0/41 | 0% | 95.3% |
| ... | theta | 0.0664 | 0.0664 | 42/43 | 0/41 | 0% | 97.7% |
| ... | l.alpha | 0.0678 | 0.0678 | 21/43 | 19/41 | 46.3% | 48.8% |
| ... | h.alpha | 0.1424 | 0.1424 | 0/43 | 40/41 | 97.6% | 0% |
| ... | beta | 0.1032 | 0.1002 | 0/43 | 40/41 | 97.6% | 0% |
| ... | gamma | 0.1050 | 0.1050 | 0/43 | 40/41 | 97.6% | 0% |
| Fp1 | delta | 0.0733 | 0.0776 | 41/43 | 0/41 | 0% | 95.3% |
| ... | theta | 0.0723 | 0.0753 | 42/43 | 0/41 | 0% | 97.7% |
| ... | l.alpha | 0.1281 | 0.1242 | 1/43 | 41/41 | 100% | 2.3% |
| ... | h.alpha | 0.0739 | 0.0769 | 42/43 | 0/41 | 0% | 97.7% |
| ... | beta | 0.1080 | 0.1029 | 1/43 | 40/41 | 97.6% | 2.3% |
| ... | gamma | 0.0690 | 0.0690 | 42/43 | 0/41 | 0% | 97.7% |
| F4 | delta | 0.0805 | 0.0767 | 41/43 | 1/41 | 2.4% | 95.3% |
| ... | theta | 0.0702 | 0.0758 | 40/43 | 0/41 | 0% | 93.0% |
| ... | l.alpha | 0.1322 | 0.1237 | 0/43 | 41/41 | 100% | 0% |
| ... | h.alpha | 0.0753 | 0.0763 | 42/43 | 0/41 | 0% | 97.7% |
| ... | beta | 0.0567 | 0.0567 | 42/43 | 1/41 | 2.4% | 97.7% |
| ... | gamma | 0.0727 | 0.0706 | 41/43 | 0/41 | 0% | 95.3% |
| F3 | delta | 0.0716 | 0.0762 | 41/43 | 0/41 | 0% | 95.3% |
| ... | theta | 0.0807 | 0.0775 | 42/43 | 1/41 | 2.4% | 97.7% |
| ... | l.alpha | 0.1223 | 0.1223 | 0/43 | 40/41 | 97.6% | 0% |
| ... | h.alpha | 0.0784 | 0.0693 | 22/43 | 22/41 | 53.7% | 51.2% |
| ... | beta | 0.1073 | 0.1072 | 0/43 | 40/41 | 97.6% | 0% |
| ... | gamma | 0.1014 | 0.1000 | 0/43 | 40/41 | 97.6% | 0% |
| C4 | delta | 0.0767 | 0.0732 | 42/43 | 1/41 | 2.4% | 97.7% |
| ... | theta | 0.0672 | 0.0738 | 42/43 | 0/41 | 0% | 97.7% |
| ... | l.alpha | 0.1177 | 0.1177 | 0/43 | 40/41 | 97.6% | 0% |
| ... | h.alpha | 0.1235 | 0.1235 | 0/43 | 41/41 | 100% | 0% |
| ... | beta | 0.1130 | 0.1079 | 1/43 | 41/41 | 100% | 2.3% |
| ... | gamma | 0.0589 | 0.0589 | 42/43 | 0/41 | 0% | 97.7% |
| C3 | delta | 0.0786 | 0.0722 | 42/43 | 1/41 | 2.4% | 97.7% |
| ... | theta | 0.1193 | 0.1193 | 0/43 | 20/41 | 48.8% | 0% |
| ... | l.alpha | 0.0730 | 0.0748 | 40/43 | 0/41 | 0% | 93.0% |
| ... | h.alpha | 0.1119 | 0.1119 | 0/43 | 40/41 | 97.6% | 0% |
| ... | beta | 0.0694 | 0.0740 | 40/43 | 0/41 | 0% | 93.0% |
| ... | gamma | 0.1096 | 0.1025 | 1/43 | 19/41 | 46.3% | 2.3% |
| P4 | **delta** | 0.1250 | 0.1250 | 42/43 | 19/41 | 46.3% | 97.7% |
| ... | theta | 0.0703 | 0.0597 | 42/43 | 1/41 | 2.4% | 97.7% |
| ... | l.alpha | 0.1231 | 0.1214 | 1/43 | 41/41 | 100% | 2.3% |
| ... | h.alpha | 0.0745 | 0.0714 | 41/43 | 0/41 | 0% | 95.3% |
| ... | beta | 0.1072 | 0.1072 | 0/43 | 40/41 | 97.6% | 0% |
| ... | gamma | 0.1015 | 0.1015 | 0/43 | 40/41 | 97.6% | 0% |
| P3 | delta | 0.0750 | 0.0750 | 42/43 | 0/41 | 0% | 97.7% |
| ... | theta | 0.0697 | 0.0753 | 21/43 | 21/41 | 51.2% | 48.8% |
| ... | **l.alpha** | 0.0658 | 0.0750 | 42/43 | 20/41 | 48.8% | 97.7% |
| ... | h.alpha | 0.1201 | 0.1190 | 0/43 | 40/41 | 97.6% | 0% |
| ... | beta | 0.1075 | 0.1075 | 0/43 | 40/41 | 100% | 0% |
| ... | gamma | 0.1032 | 0.1032 | 0/43 | 40/41 | 97.6% | 0% |
| O2 | delta | 0.1207 | 0.1207 | 22/43 | 20/49 | 48.8% | 51.2% |
| ... | theta | 0.0761 | 0.0722 | 42/43 | 1/41 | 2.4% | 97.7% |
| ... | l.alpha | 0.0713 | 0.0745 | 42/43 | 0/41 | 0% | 97.7% |
| ... | h.alpha | 0.1171 | 0.1160 | 0/43 | 40/41 | 97.6% | 0% |
| ... | beta | 0.0721 | 0.0656 | 42/43 | 1/41 | 2.4% | 97.7% |
| ... | gamma | 0.1108 | 0.1108 | 0/43 | 40/41 | 97.6% | 0% |
| O1 | delta | 0.1272 | 0.1272 | 0/43 | 40/41 | 97.6% | 0% |
| ... | theta | 0.0736 | 0.0675 | 42/43 | 1/41 | 2.4% | 97.7% |
| ... | l.alpha | 0.1136 | 0.1136 | 0/43 | 40/41 | 97.6% | 0% |

***Table 11.2:*** *Leave-one-out method applied on the $r_g$-values for all nodes and all frequency bands. Promising results are marked in bold.*

| Node | fr. band | thr. spec. | thr. sens. | epi class. as epi | contr class. as contr | spec. | sens. |
|---|---|---|---|---|---|---|---|
| ... | h.alpha | 0.0710 | 0.0710 | 42/43 | 0/41 | 0% | 97.7% |
| ... | beta | 0.0700 | 0.0589 | 41/43 | 1/41 | 2.4% | 95.3% |
| ... | gamma | 0.0730 | 0.0695 | 42/43 | 1/41 | 2.4% | 97.7% |
| F8 | delta | 0.0714 | 0.0645 | 42/43 | 1/41 | 2.4% | 97.7% |
| ... | theta | 0.1476 | 0.1476 | 0/43 | 40/41 | 97.6% | 0% |
| ... | l.alpha | 0.1203 | 0.1172 | 1/43 | 41/41 | 100% | 2.3% |
| ... | h.alpha | 0.0637 | 0.0761 | 36/43 | 0/41 | 0% | 83.7% |
| ... | beta | 0.0748 | 0.0720 | 21/43 | 0/41 | 0% | 48.8% |
| ... | gamma | 0.0714 | 0.0622 | 42/43 | 1/41 | 2.4% | 97.7% |
| F7 | delta | 0.1241 | 0.1210 | 1/43 | 40/41 | 97.6% | 2.3% |
| ... | theta | 0.1200 | 0.1051 | 1/43 | 40/41 | 97.6% | 2.3% |
| ... | l.alpha | 0.1167 | 0.1167 | 0/43 | 41/41 | 100% | 0% |
| ... | h.alpha | 00814 | 0.0697 | 42/43 | 1/41 | 2.4% | 97.7% |
| ... | beta | 0.0670 | 0.0696 | 42/43 | 0/41 | 0% | 97.7% |
| ... | **gamma** | 0.1128 | 0.1128 | 21/43 | 40/41 | 97.6% | 48.8% |
| T4 | delta | 0.0753 | 0.0753 | 21/43 | 0/41 | 51.2% | 48.8% |
| ... | theta | 0.0600 | 0.0701 | 41/43 | 0/41 | 0% | 95.3% |
| ... | l.alpha | 0.1131 | 0.1066 | 0/43 | 21/41 | 51.2% | 0% |
| ... | h.alpha | 0.1189 | 0.1189 | 21/43 | 20/41 | 48.8% | 48.8% |
| ... | beta | 0.1051 | 0.0981 | 1/43 | 40/41 | 97.6% | 2.3% |
| ... | gamma | 0.0971 | 0.0959 | 0/43 | 40/41 | 97.6% | 0% |
| T3 | delta | 0.0762 | 0.0785 | 40/43 | 0/41 | 0% | 93.0% |
| ... | theta | 0.1182 | 0.1112 | 1/43 | 41/41 | 100% | 23% |
| ... | l.alpha | 0.1151 | 0.1112 | 1/43 | 40/41 | 97.6% | 2.3% |
| ... | h.alpha | 0.0680 | 0.0680 | 42/43 | 0/41 | 0% | 97.7% |
| ... | beta | 0.1124 | 0.1077 | 1/43 | 40/41 | 97.6% | 2.3% |
| ... | gamma | 0.0733 | 0.0710 | 42/43 | 1/41 | 2.4% | 97.7% |
| T6 | delta | 0.1195 | 0.1195 | 0/43 | 40/41 | 97.6% | 0% |
| ... | theta | 0.0722 | 0.0766 | 42/43 | 0/41 | 0% | 97.7% |
| ... | l.alpha | 0.0608 | 0.0608 | 42/43 | 1/41 | 2.4% | 97.7% |
| ... | h.alpha | 0.0741 | 0.0683 | 41/43 | 0/41 | 0% | 95.3% |
| ... | beta | 0.0697 | 0.0697 | 42/43 | 0/41 | 0% | 97.7% |
| ... | gamma | 0.1038 | 0.1038 | 0/43 | 40/41 | 97.6% | 0% |
| T5 | delta | 0.0772 | 0.0777 | 40/43 | 0/41 | 0% | 93.0% |
| ... | theta | 0.0657 | 0.0725 | 41/43 | 0/41 | 0% | 95.3% |
| ... | l.alpha | 0.1148 | 0.1073 | 0/43 | 40/41 | 97.6% | 0% |
| ... | **h.alpha** | 0.1161 | 0.1149 | 22/43 | 40/41 | 97.6% | 51.2% |
| ... | beta | 0.1078 | 0.0988 | 22/43 | 21/41 | 51.2% | 51.2% |
| ... | gamma | 0.0703 | 0.0703 | 42/43 | 0/41 | 0% | 97.7% |
| Fz | **delta** | 0.1120 | 0.1120 | 21/43 | 40/41 | 97.6% | 48.8% |
| ... | theta | 0.0755 | 0.0669 | 42/43 | 1/41 | 2.4% | 97.7% |
| ... | l.alpha | 0.0808 | 0.0542 | 42/43 | 1/41 | 2.4% | 97.7% |
| ... | h.alpha | 0.1143 | 0.1065 | 1/43 | 41/41 | 100% | 2.3% |
| ... | beta | 0.0657 | 0.0696 | 41/43 | 0/41 | 0% | 95.3% |
| ... | gamma | 0.1037 | 0.1037 | 0/43 | 40/41 | 97.6% | 0% |
| Cz | delta | 0.0698 | 0.0698 | 42/43 | 1/43 | 2.4% | 97.7% |
| ... | theta | 0.1115 | 0.1049 | 1/43 | 41/41 | 100% | 2.3% |
| ... | l.alpha | 0.0612 | 0.0612 | 42/43 | 0/41 | 0% | 97.7% |
| ... | h.alpha | 0.0719 | 0.0742 | 40/43 | 0/41 | 0% | 93.0% |
| ... | beta | 0.1067 | 0.1067 | 1/43 | 41/41 | 100% | 2.3% |
| ... | gamma | 0.1016 | 0.1016 | 0/43 | 40/41 | 97.6% | 0% |
| Pz | delta | 0.0669 | 0.0753 | 40/43 | 0/41 | 0% | 93.3% |
| ... | theta | 0.1073 | 0.1073 | 0/43 | 40/41 | 97.6% | 0% |
| ... | l.alpha | 0.0765 | 0.0730 | 42/43 | 1/41 | 2.4% | 97.7% |
| ... | h.alpha | 0.1102 | 0.1102 | 0/43 | 40/41 | 97.6% | 0% |
| ... | beta | 0.0661 | 0.0661 | 42/43 | 0/41 | 0% | 97.7% |
| ... | gamma | 0.0998 | 0.0984 | 0/43 | 40/41 | 97.6% | 0% |

***Table 11.2:*** *Part 2 of the leave-one-out method part applied on the $r_g$-values for all nodes and all frequency bands. Promising results are marked in bold.*